NANO LETTERS

pubs.acs.org/NanoLett Letter

Ultrafast Modulation of Stacking Orders in vdW Layers by Photoinduced Pseudosliding of Ferroelectric Monolayer

Meng Niu, Nian-Ke Chen,* Bai-Qian Wang, Shun-Yao Qin, Yu-Ting Huang, Hong-Bo Sun, Shengbai Zhang, and Xian-Bin Li*

Cite This: https://doi.org/10.1021/acs.nanolett.5c02237 Read Online

ACCESS | Metrics & More | Article Recommendations | Supporting Information

ABSTRACT: Precise control of stacking orders in van der Waals (vdW) heterostructures not only generates novel quantum phenomena but also promises applications in memory and computing devices. However, achieving robust control of the stacking order in vdW heterostructures remains a significant challenge. In this work, TDDFT-MD simulations reveal a photoinduced ultrafast and nonvolatile in-plane structural transition in ferroelectric antimonene. This transition can modify the stacking order in vdW heterostructures based on antimonene. It resembles a sliding effect but retains the geometric center of the antimonene layer and is therefore termed pseudosliding. Furthermore, optical-property switching via pseudosliding is also demonstrated in an Sb/SnSe vdW heterostructure. The present work proposes a new strategy for ultrafast and robust control of stacking orders in vdW heterostructures, leveraging ferroelectric monolayers with an in-plane Peierls distortion.

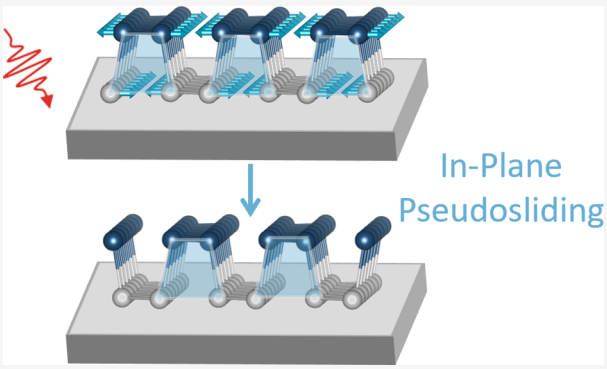

KEYWORDS: *stacking order, pseudosliding, photoinduced transition, nonvolatile memory, time-dependent density functional theory*

Two-dimensional van der Waals (vdW) materials can be stacked with high flexibility, bringing about a wide range of applications in electronics,[1−4] photonics,[5,6] sensors,[7,8] and other fields. The stacking engineering of vdW layers or heterostructures—including sliding, twisting, and lattice mismatches of 2D materials—gives rise to numerous exotic phenomena,[9] such as sliding ferroelectricity,[10] magnetic state switching,[11] magic-angle superconductivity,[12] and moiré superlattices.[13,14] Controlling the stacking order serves as a fundamental cornerstone for constructing such vdW heterostructures. Furthermore, the fast and reversible manipulation of the stacking order, such as sliding ferroelectricity, enables nonvolatile memory or computing applications with low power consumption, fast speed, and excellent endurance.[15] The stacking or sliding order of vdW layers can be controlled through various manners such as electrical fields,[16] chemical means,[17] mechanical stress,[18] and optical pumping.[19] Among them, light-induced sliding holds the advantages of being ultrafast, remote-controllable, and noninvasive. Recent experiments have already revealed that femtosecond (fs) lasers can induce strong electron−phonon coupling in 2D, 1D, and twist-angle vdW heterolayers and, thus, effectively modulate the electronic and structural dynamics.[20−22] However, light-induced sliding of the vdW layers usually depends on the activation of shear phonon modes.[23−25] This mechanism not only is characterized by a relatively weak driving force it generates but also necessitates strong interlayer coupling within specific vdW layers, making precise control of their relative sliding difficult. Therefore, a new strategy to precisely control stacking orders in vdW heterostructures is urgently required to promote their applications.

Materials with Peierls distortions have been demonstrated to generally exhibit structural responses to the ultrafast laser excitation via the mechanism of displacive excitation of coherent phonons (DECP).[26,27] Therefore, 2D materials exhibiting in-plane Peierls distortions coupled with an adjacent substrate layer could potentially enable ultrafast stacking-order modulations through photoinduced lateral displacements. The recently demonstrated 2D elemental ferroelectrics (such as arsenene, antimonene, and bismuthene)[28−30] with in-plane Peierls distortions may meet the demands. If these ferroelectric monolayers are used as building blocks in vdW heterostructures, then the stacking order could be precisely controlled by light.

In this work, taking the ferroelectric α-antimonene (i.e., a monolayer Sb) as an example, time-dependent density functional theory molecular dynamics (TDDFT-MD) demon-

Received: April 18, 2025
Revised: July 6, 2025
Accepted: July 28, 2025

https://doi.org/10.1021/acs.nanolett.5c02237
Nano Lett. XXXX, XXX, XXX−XXX

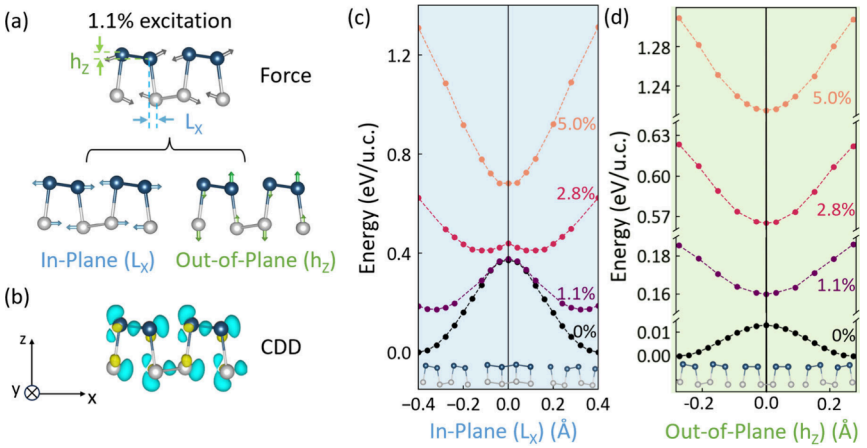

Figure 1. (a) Side view of the atomic structure of free-standing α-antimonene, with arrows indicating instant forces acting on atoms under a 1.1% excitation intensity. The bottom panels show the projection of atomic forces along the in-plane and out-of-plane directions. Two structural parameters, L_X and h_Z, are also noted. (b) Instant charge density difference (CDD) under the 1.1% excitation, i.e., $\Delta\rho = \rho_{\text{excitation}} - \rho_{\text{ground}}$. The isosurface is 0.0005 e/a_0^3, where a_0 is the Bohr radius. Yellow and blue areas represent regions of increased and decreased charge density, respectively. Excitation intensity-dependent potential energy surfaces (PESs) along (c) in-plane (L_X) and (d) out-of-plane (h_Z) directions. The black, purple, red, and orange dotted lines correspond to the 0% (ground state) and 1.1%, 2.8%, and 5.0% excitation intensities, respectively.

strates that the ultrafast laser can control the lateral movements of atoms in α-antimonene to realize the nonvolatile structure transition. As a result, a pseudosliding effect is achieved; that is, the stacking order between α-antimonene and a substrate layer is changed, but the geometrical center of α-antimonene remains unchanged. Analyses on potential energy surfaces (PES) demonstrate that the driving force for the lateral motions is due to the DECP effect. The nonvolatility, which is the key to controlling stacking orders, is attributed to the ultrafast dephasing of lattice coherence and the deexcitation of excited carriers via electron−phonon coupling effects. Furthermore, a vdW heterostructure constructed by α-antimonene and monolayer SnSe is used to demonstrate that the pseudosliding-induced stacking-order switching can indeed modulate the optical property of the heterostructure. This study proposes an optical approach to manipulate the stacking order in antimonene-based vdW heterostructures, targeting advanced optoelectronic applications.

The TDDFT-MD calculations are performed using the time-dependent *ab initio* package (TDAP) as implemented in SIESTA[31] with norm-conserving Troullier−Martins pseudopotentials,[32] the PBE functional,[33] and the NVE ensemble. The plane wave energy cutoff is 200 Ry, and the local basis set with double-ζ-polarized orbitals is employed. The coupling between atomic and electronic motions is governed by the Ehrenfest approximation.[34] The rationality of the approximation is further discussed in **Note 1** of the Supporting Information (SI). In fact, the method we used here has successfully explained various experimental observations for photoinduced structure evolution of different materials on the time scale from 600 to 3000 fs.[25,35−41] The constructed supercell slabs in this study are periodic in the x−y plane and are separated by a vacuum of 25 Å in the z-direction (perpendicular to the plane) to avoid interaction between periodic slab images. The time step is 0.024 fs, and the equilibrium state of *ab initio* MD at 300 K is used as the input. In TDDFT-MD, we use a 144-atom Sb supercell ($6 \times 6 \times 1$) and the Γ point for Brillouin zone integration. We simulate the excitation of the electrons by changing the occupation of the corresponding Kohn-Sham states involved in the photoexcitation.[42] The photoexcitation process is simulated by promoting electrons from the valence band to the conduction band within the Sb layer.[43,44] The quantity of the excitation intensity is defined as the ratio of excited electrons to the number of valence electrons of Sb layer. To calculate the optical properties of the Sb/SnSe heterostructure, the frequency-dependent dielectric constants[45] are calculated with the generalized gradient approximation by the Vienna *Ab initio* Simulation Package.[46] The van der Waals interactions are incorporated in the optical-property calculations with the DFT-D2 method.[47]

The structure of free-standing α-antimonene is similar to that of monolayer black phosphorus with in-plane distortions, but the Sb layer also exhibits out-of-plane distortions.[29] To quantitatively describe the out-of-plane (along z direction) and in-plane (along x direction) structural distortions, two structural parameters are defined, namely, h_Z and L_X, as shown in Figure 1a. The h_Z value of black phosphorus is zero, indicating no out-of-plane distortion, while that of antimonene is nonzero, suggesting the presence of out-of-plane distortion. Another key parameter in α-antimonene is L_X, which represents the average horizontal distance between the atoms in the upper (blue) and lower (gray color) sublayers. To illustrate the response of the Sb layer to photoexcitation, the instant forces on atoms in the excited state are analyzed (see the arrows in Figure 1a). These forces can be projected onto in-plane and out-of-plane directions. In other words, both the in-plane and the out-of-plane structure distortions can be modulated by light. The origin of the driving force can be understood by the charge density difference (CDD) between the excited and ground states, as shown in Figure 1b. The excitation mainly reduces the number of lone-pair and in-plane bonding electrons (blue areas in Figure 1b). Therefore, the repulsion between adjacent lone pairs and the attraction between the bonding atoms are both weakened. As a result, the adjacent nonbonding atoms have a tendency to get closer, and the bonding atoms will be apart, which is consistent with the in-plane directions of instant atomic forces under the excitation; see Figure 1a. Further analyses on partial density of states of Sb, forces under different excitations, and their time evolutions are shown in Figures S1 and S2 in the SI, Note 2.

https://doi.org/10.1021/acs.nanolett.5c02237
Nano Lett. XXXX, XXX, XXX−XXX

Next, the potential energy surfaces (PESs) of free-standing α-antimonene at different excitation intensities are calculated (Figures 1c,d). The PES for the in-plane and out-of-plane motions is plotted with L_X and h_Z, respectively. The ground-state PESs in both directions exhibit typical double-well landscapes, which are characteristic of Peierls distortions. Considering the ferroelectricity of α-antimonene, the two minima of one PES represent two antiparallel polarized states. As the excitation intensity increases, the minima of the PES gradually move closer, indicating that distortions are reduced by the excitation. The atomic forces and the PESs indicate that the coherent atom motions along in-plane or out-of-plane directions will be activated in the typical DECP manner.[26] These results align with previous reports that photoexcitation drives the evolution of Peierls-distorted structures from low-symmetry to high-symmetry states.[37,43,48]

Nevertheless, the transition energy barrier between two polarized states in the in-plane PES (370 meV at 0% excitation) is significantly higher than that in the out-of-plane PES (13 meV at 0% excitation). The reason is that the in-plane structural transition involves the breaking and reforming of chemical bonds (see the inset in Figure 1c), while the out-of-plane transition only requires the rotation of chemical bonds (see the inset in Figure 1d). For example, for the out-of-plane direction (h_Z), a relatively small excitation intensity, such as 1.1%, is sufficient to induce the transition from one polarization state to another opposite polarization state. In contrast, for the in-plane direction (L_X), the PES maintains a double-well landscape at excitation intensities of 1.1% and even 2.8% but transforms into a single-well landscape at a higher excitation intensity, such as 5.0%. As a result, a suitable excitation-intensity window, which can solely activate the out-of-plane transitions, may exist. In other words, by using an appropriate excitation, the structural transitions in the in-plane or out-of-plane directions could be precisely controlled.

To verify the preceding analyses, the dynamics of structural transitions under optical excitation are investigated by TDDFT-MD simulations. As only the in-plane (A_1^2) and out-of-plane (A_1^1) phonon modes[49] are excited (see Figure S3 in the SI, Note 3), Figures 2a–c exhibit the time evolution of L_X (in-plane) and h_Z (out-of-plane) under different excitation intensities. As expected, a relatively low excitation intensity (e.g., 1.1%) activates only the out-of-plane structural transitions as h_Z transforms from +0.2 to −0.2 Å within 900 fs, indicating its polarization switching (Figure 2a). The in-plane Peierls parameter L_X remains nearly unchanged due to the remaining large energy barrier of the PES at excitation (197 meV), as depicted in Figure 1c. As the excitation intensity increases to 2.8%, the energy barrier of the in-plane PES is significantly reduced to 28 meV, allowing L_X to cross the zero point (from −0.4 to +0.3 Å) and thus achieving the in-plane structural switching within 300 fs (Figure 2b).

Figure 2d schematically illustrates the entire structural transition process under 2.8% excitation intensity. First, the in-plane structural transition occurs, with L_X gradually changing from negative value to positive value. Then, the out-of-plane structural transition happens, in which h_Z changes from a positive value to a negative value. The in-plane structural transition does not result in an actual sliding of α-antimonene because its geometric center is retained due to the conservation of momentum. Consider further that when α-antimonene is placed on a reference vdW substrate to construct a heterostructure, such a structural transition of α-

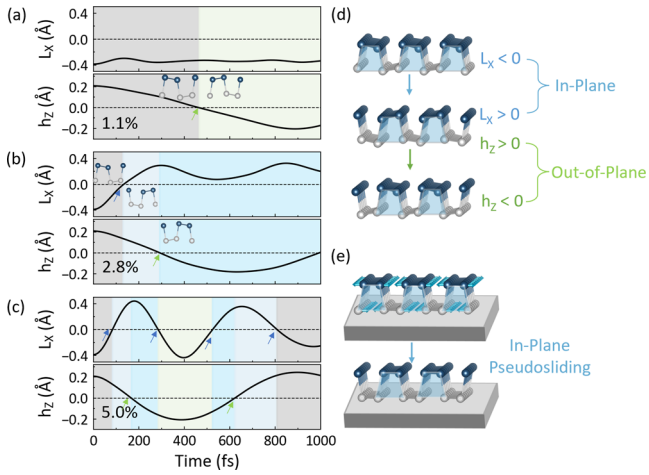

Figure 2. (a–c) Time evolutions of structural parameters L_X and h_Z under different initial excitation intensities in free-standing α-antimonene, where the arrows indicate the time points at which structural transitions from one polarization to another polarization occur. (d) Schematic illustrations of the structural transitions under the 2.8% excitation intensity. (e) Schematic illustration of the in-plane pseudosliding effect of the Sb layer on a substrate.

antimonene will change the stacking order of the heterostructure, resembling a half-lattice sliding effect along the in-plane direction (Figure 2e). Therefore, we refer to this type of in-plane structural transition as pseudosliding on a substrate. Note that the pseudosliding observed under the 2.8% excitation intensity is a nonvolatile process in the simulation, indicating that the switched structure would be retained. The calculations are also performed using supercells of various sizes, and the conclusions of the pseudosliding of the Sb layer remain valid (see Figure S4 in the SI, Note 4).

If the excitation intensity is as large as 5.0%, then both the in-plane and out-of-plane PESs will transform into a single-well PES (Figures 1c,d). Subsequently, the structure oscillates back and forth in both directions, losing precise control on the ultrafast time scale (Figure 2c). Therefore, the nonvolatility of the in-plane pseudosliding under the 2.8% excitation intensity is crucial for the precise control of stacking orders. The underlying mechanism of nonvolatility thus warrants a more insightful understanding. First, the PES-governed transitions in Figures 1 and 2 clearly revealed a strong dependence on excitation intensities. To further elucidate this, the time evolution of the excitation intensity during the TDDFT-MD simulations is evaluated (Figure 3b and Figure S5 in the SI, Note 5), which gradually decreases due to the recombination of carriers. The PES values for the decreased excitation intensities are calculated and compared (Figure 3a). Obviously, the initial excitation (2.8% at 0 fs) provides a large driving force for the structural switching. Thereafter, as the excitation decreases with time, the energy barrier rises again, preventing the structure from switching, while for a larger excitation of 5%, the excitation intensity remains large and the barrier also remains small during the whole simulation, suggesting the nonstop transition (Figure 3c). Second, according to previous reports,[43,48] coherent motions are necessary for ultrafast structural transitions without the conventional nucleation-and-growth process. To measure the coherence of atomic motions, a parameter of correlation degree defined by the Pearson correlation coefficient (see **Note 6** in the SI for more details) is then calculated (Figure 3b,c).

https://doi.org/10.1021/acs.nanolett.5c02237
Nano Lett. XXXX, XXX, XXX−XXX

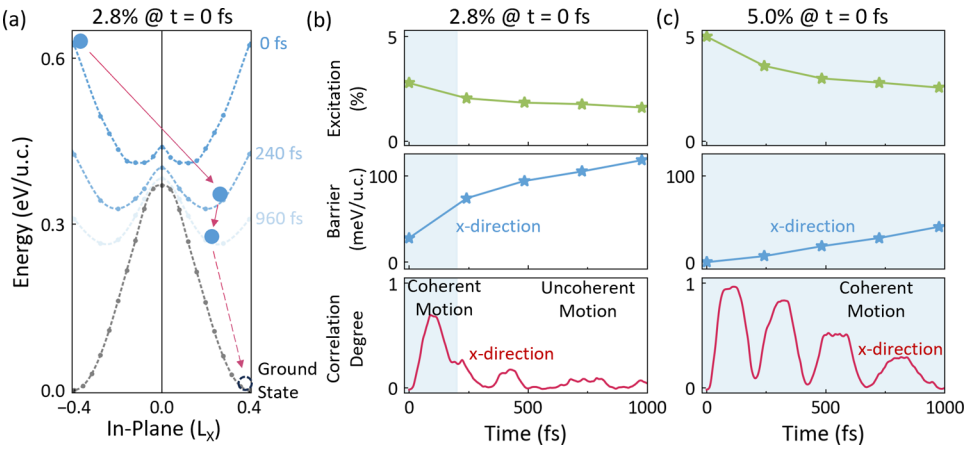

Figure 3. (a) Time evolution of the PES and schematic diagram of the nonvolatile structural transition under 2.8% excitation at 0 fs in α-antimonene. Time evolutions of the excitation intensity, the energy barrier of in-plane PES, and the correlation degree of atom motions, under two initial excitation intensities of (b) 2.8% and (c) 5% at 0 fs.

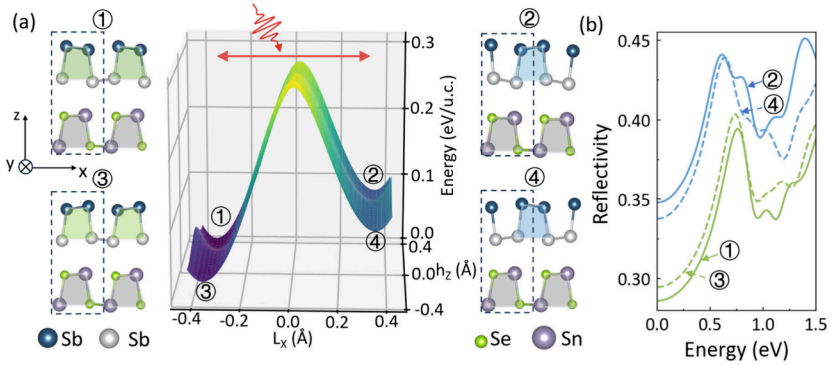

Figure 4. (a) Side view of four stacking configurations of the Sb/SnSe vdW heterostructure and the related potential energy surface. (b) The reflectivity of the four stacking states calculated based on the zigzag direction (i.e., the y direction) dielectric constants.

Here, the correlation degree of 1 indicates that atomic motions are completely positively correlated (coherent), while the correlation degree of 0 signifies that atomic motions are entirely uncorrelated (uncoherent). For the 2.8% excitation (Figure 3b), the atomic motion is highly coherent at the beginning, such as at ∼100 fs. Subsequently, after the in-plane (L_X) structural transition, such as >300 fs, the coherence of atomic motions has significantly decreased due to electron−phonon coupling. The coherence of atomic motions can also be confirmed by the time evolution of average momentum along x, y, and z directions (Figure S6 in the SI, Note 5). As a result, the structure cannot switch back, enabling the nonvolatility of the pseudosliding. In contrast, when the excitation intensity is 5.0%, the atomic motions remain coherent throughout the whole simulation (1000 fs), although with a gradually decaying amplitude (Figure 3c). Meanwhile, the structure undergoes back-and-forth oscillations, as shown in Figure 2c. Therefore, the deexcitation effect and rapid dephasing of lattice coherence are the key factors contributing to the nonvolatile structural transition.

Finally, using the monolayer SnSe as a substrate, an Sb/SnSe vdW heterostructure is constructed to demonstrate the ability of optical-property modulation by the α-antimonene pseudosliding. The proposal is reasonable, as the Sb/SnSe heterostructure has been experimentally fabricated in the previous research.[50] Additionally, by applying appropriate photonic energy, the larger bandgap of SnSe compared to that of Sb ensures that the SnSe layer remains basically undisturbed during the pseudosliding of the Sb layer (**Note 7** in the SI). Figure 4a shows four possible stacking orders based on the in-plane (L_X) and out-of-plane (h_Z) structural transitions. Compared to the symmetric PES of the free-standing Sb layer, the asymmetric PES of the Sb layer in Figure 4a is due to symmetry breaking by the substrate SnSe layer. The switching from states ①/③ to states ②/④ corresponds to the in-plane structural transition of α-antimonene, while the switching from states ①/② to states ③/④ corresponds to the out-of-plane structural transition of the Sb layer. Detailed pictures of the transitions between different stacking orders in the Sb/SnSe vdW heterostructure and their corresponding energy barriers are further discussed in SI, Note 7. Then, the optical reflectivities of the four states are calculated (Figure 4b). The reflectivity of states ② and ④ is clearly distinguished from that of states ① and ③ in the frequency ranges of [0−0.6 eV] and [0.7−1.2 eV]. The out-of-plane structural transition between ② and ④ or between ① and ③ does not affect the reflectivity much. In other words, the pseudosliding from states ①/③ to states ②/④ results in significant optical property modulation, displaying potential in optical memory or computing applications.

Note that the monolayer SnSe is chosen as a substrate because its lattice parameters are close to those of α-antimonene. In fact, due to the flexibility in constructing vdW heterostructures,[51,52] other substrates can also be

https://doi.org/10.1021/acs.nanolett.5c02237
Nano Lett. XXXX, XXX, XXX−XXX

employed. On the other hand, as long as the bandgap (E_g) of the substrate layer is larger than that of the Sb layer, a laser pulse with proper photonic energy in a range of E_g(Sb) < E(photon) < E_g(the substrate layer) can selectively excite the Sb layer. Furthermore, the photoexcitation-induced pseudosliding of the Sb layer on the monolayer boron nitride (BN) is also demonstrated; see **Note 8** in the SI.

In conclusion, we propose a novel strategy, termed pseudosliding, to control stacking orders in vdW heterostructures with ultrafast speed by light. Taking α-antimonene with in-plane Peierls distortion as an example, TDDFT-MD studies demonstrate that nonvolatile in-plane structural transitions can be achieved within 300 fs by ultrafast photoexcitation. The driving force of the transition is the DECP effect, and the nonvolatility is due to the deexcitation effect and rapid dephasing of lattice coherence. Such an in-plane transition of the Sb layer can alter the stacking order in the Sb-based vdW heterostructure, resembling a half-lattice sliding effect (i.e., pseudosliding). Furthermore, optical properties, such as reflectivity, can be modulated accordingly. Although this work focuses on antimonene, it should also be applied to other 2D materials with in-plane Peierls distortions. The pseudosliding methodology in this work offers a potential pathway for tuning stacking orders precisely in vdW heterostructures, which may facilitate explorations of unconventional quantum states and optical memory/computing applications.

■ ASSOCIATED CONTENT

Supporting Information

The Supporting Information is available free of charge at https://pubs.acs.org/doi/10.1021/acs.nanolett.5c02237.

Details of the Ehrenfest dynamics, forces on atoms under excitation, the projected phonon mode intensity, supercell size for TDDFT-MDs, evolution of excitation intensity and atomic momentum, the explanation of the correlation degree, the ultrafast pseudosliding of Sb on a SnSe substrate, and the ultrafast pseudosliding of Sb on a BN substrate (PDF)

■ AUTHOR INFORMATION

Corresponding Authors

Nian-Ke Chen − *State Key Laboratory of Integrated Optoelectronics, College of Electronic Science and Engineering, Jilin University, Changchun 130012, China*; Email: chennianke@jlu.edu.cn

Xian-Bin Li − *State Key Laboratory of Integrated Optoelectronics, College of Electronic Science and Engineering, Jilin University, Changchun 130012, China*; orcid.org/0000-0002-0046-2016; Email: lixianbin@jlu.edu.cn

Authors

Meng Niu − *State Key Laboratory of Integrated Optoelectronics, College of Electronic Science and Engineering, Jilin University, Changchun 130012, China*

Bai-Qian Wang − *State Key Laboratory of Integrated Optoelectronics, College of Electronic Science and Engineering, Jilin University, Changchun 130012, China*

Shun-Yao Qin − *State Key Laboratory of Integrated Optoelectronics, College of Electronic Science and Engineering, Jilin University, Changchun 130012, China*

Yu-Ting Huang − *State Key Laboratory of Integrated Optoelectronics, College of Electronic Science and Engineering, Jilin University, Changchun 130012, China*; orcid.org/0009-0005-9208-2780

Hong-Bo Sun − *State Key Lab of Precision Measurement Technology and Instruments, Department of Precision Instrument, Tsinghua University, Beijing 100084, China*

Shengbai Zhang − *Department of Physics, Applied Physics, and Astronomy, Rensselaer Polytechnic Institute, Troy, New York 12180, United States*

Complete contact information is available at: https://pubs.acs.org/10.1021/acs.nanolett.5c02237

Notes

The authors declare no competing financial interest.

■ ACKNOWLEDGMENTS

Work in China was supported by the National Science and Technology Major Project (Grant No. 2022ZD0117600), the National Natural Science Foundation of China (Grant Nos. 12274180, 12274172), the Science and Technology Development Plan Project of Changchun, China (Grant No. 2024GZZ07), and China Postdoctoral Science Foundation (Grant No. BX20240136). The High-Performance Computing Center (HPCC) at Jilin University for computational resources is also acknowledged. We are also very grateful to Dr. Chao Lian for his valuable suggestions.

■ REFERENCES

(1) Wang, C.; You, L.; Cobden, D.; Wang, J. Towards two-dimensional van der Waals ferroelectrics. *Nat. Mater.* **2023**, *22*, 542−552.

(2) Wang, Z.; Zhou, X.; Liu, X.; Qiu, A.; Gao, C.; Yuan, Y.; Jing, Y.; Zhang, D.; Li, W.; Luo, H.; et al. Van der Waals ferroelectric transistors: the all-round artificial synapses for high-precision neuromorphic computing. *Chip* **2023**, *2*, No. 100044.

(3) Yang, X.; Li, J.; Song, R.; Zhao, B.; Tang, J.; Kong, L.; Huang, H.; Zhang, Z.; Liao, L.; Liu, Y.; et al. Highly reproducible van der Waals integration of two-dimensional electronics on the wafer scale. *Nat. Nanotechnol.* **2023**, *18*, 471−478.

(4) Su, Z.-J.; Xuan, Z.-H.; Liu, J.; Kang, Y.; Liu, C.-S.; Zuo, C.-J. Sub-femto-Joule energy consumption memory device based on van der Waals heterostructure for in-memory computing. *Chip* **2022**, *1*, No. 100014.

(5) Meng, Y.; Feng, J.; Han, S.; Xu, Z.; Mao, W.; Zhang, T.; Kim, J. S.; Roh, I.; Zhao, Y.; Kim, D.-H.; et al. Photonic van der Waals integration from 2D materials to 3D nanomembranes. *Nat. Rev. Mater.* **2023**, *8*, 498−517.

(6) Wu, D.; Guo, C.; Zeng, L.; Ren, X.; Shi, Z.; Wen, L.; Chen, Q.; Zhang, M.; Li, X. J.; Shan, C.-X.; et al. Phase-controlled van der Waals growth of wafer-scale 2D $MoTe_2$ layers for integrated high-sensitivity broadband infrared photodetection. *Light Sci. Appl.* **2023**, *12*, 5.

(7) Hu, A.-Q.; Liu, Q.-L.; Guo, X. Carrier localization enhanced high responsivity in graphene/semiconductor photodetectors. *Chip* **2022**, *1*, No. 100006.

(8) Yoon, H. H.; Fernandez, H. A.; Nigmatulin, F.; Cai, W.; Yang, Z.; Cui, H.; Ahmed, F.; Cui, X.; Uddin, M. G.; Minot, E. D.; et al. Miniaturized spectrometers with a tunable van der Waals junction. *Science* **2022**, *378*, 296−299.

(9) Fox, C.; Mao, Y.; Zhang, X.; Wang, Y.; Xiao, J. Stacking Order Engineering of Two-Dimensional Materials and Device Applications. *Chem. Rev.* **2024**, *124*, 1862−1898.

(10) Wu, M.; Li, J. Sliding ferroelectricity in 2D van der Waals materials: Related physics and future opportunities. *Proc. Natl. Acad. Sci. U.S.A.* **2021**, *118*, No. e2115703118.

(11) Song, T.; Fei, Z.; Yankowitz, M.; Lin, Z.; Jiang, Q.; Hwangbo, K.; Zhang, Q.; Sun, B.; Taniguchi, T.; Watanabe, K.; et al. Switching 2D magnetic states via pressure tuning of layer stacking. *Nat. Mater.* **2019**, *18*, 1298−1302.
(12) Hao, Z.; Zimmerman, A. M.; Ledwith, P.; Khalaf, E.; Najafabadi, D. H.; Watanabe, K.; Taniguchi, T.; Vishwanath, A.; Kim, P. Electric field−tunable superconductivity in alternating-twist magic-angle trilayer graphene. *Science* **2021**, *371*, 1133−1138.
(13) Chen, G.; Sharpe, A. L.; Gallagher, P.; Rosen, I. T.; Fox, E. J.; Jiang, L.; Lyu, B.; Li, H.; Watanabe, K.; Taniguchi, T.; et al. Signatures of tunable superconductivity in a trilayer graphene moiré superlattice. *Nature* **2019**, *572*, 215−219.
(14) Xiong, R.; Nie, J. H.; Brantly, S. L.; Hays, P.; Sailus, R.; Watanabe, K.; Taniguchi, T.; Tongay, S.; Jin, C. Correlated insulator of excitons in WSe_2/WS_2 moiré superlattices. *Science* **2023**, *380*, 860−864.
(15) Bian, R.; He, R.; Pan, E.; Li, Z.; Cao, G.; Meng, P.; Chen, J.; Liu, Q.; Zhong, Z.; Li, W.; et al. Developing fatigue-resistant ferroelectrics using interlayer sliding switching. *Science* **2024**, *385*, 57−62.
(16) Li, H.; Utama, M. I. B.; Wang, S.; Zhao, W.; Zhao, S.; Xiao, X.; Jiang, Y.; Jiang, L.; Taniguchi, T.; Watanabe, K.; et al. Global Control of Stacking-Order Phase Transition by Doping and Electric Field in Few-Layer Graphene. *Nano Lett.* **2020**, *20*, 3106−3112.
(17) Muscher, P. K.; Rehn, D. A.; Sood, A.; Lim, K.; Luo, D.; Shen, X.; Zajac, M.; Lu, F.; Mehta, A.; Li, Y.; et al. Highly Efficient Uniaxial In-Plane Stretching of a 2D Material via Ion Insertion. *Adv. Mater.* **2021**, *33*, No. 2101875.
(18) Oviedo, J. P.; Kc, S.; Lu, N.; Wang, J.; Cho, K.; Wallace, R. M.; Kim, M. J. In Situ TEM Characterization of Shear-Stress-Induced Interlayer Sliding in the Cross Section View of Molybdenum Disulfide. *ACS Nano* **2015**, *9*, 1543−1551.
(19) Zhang, M. Y.; Wang, Z. X.; Li, Y. N.; Shi, L. Y.; Wu, D.; Lin, T.; Zhang, S. J.; Liu, Y. Q.; Liu, Q. M.; Wang, J.; et al. Light-Induced Subpicosecond Lattice Symmetry Switch in $MoTe_2$. *Phys. Rev. X* **2019**, *9*, No. 021036.
(20) Sood, A.; Haber, J. B.; Carlström, J.; Peterson, E. A.; Barre, E.; Georgaras, J. D.; Reid, A. H. M.; Shen, X.; Zajac, M. E.; Regan, E. C.; et al. Bidirectional phonon emission in two-dimensional heterostructures triggered by ultrafast charge transfer. *Nat. Nanotechnol.* **2023**, *18*, 29−35.
(21) Saida, Y.; Gauthier, T.; Suzuki, H.; Ohmura, S.; Shikata, R.; Iwasaki, Y.; Noyama, G.; Kishibuchi, M.; Tanaka, Y.; Yajima, W.; et al. Photoinduced dynamics during electronic transfer from narrow to wide bandgap layers in one-dimensional heterostructured materials. *Nat. Commun.* **2024**, *15*, 4600.
(22) Luo, D.; Tang, J.; Shen, X.; Ji, F.; Yang, J.; Weathersby, S.; Kozina, M. E.; Chen, Z.; Xiao, J.; Ye, Y.; et al. Twist-Angle-Dependent Ultrafast Charge Transfer in MoS_2-Graphene van der Waals Heterostructures. *Nano Lett.* **2021**, *21*, 8051−8057.
(23) Wang, J.; Li, X.; Ma, X.; Chen, L.; Liu, J.-M.; Duan, C.-G.; Íñiguez-González, J.; Wu, D.; Yang, Y. Ultrafast Switching of Sliding Polarization and Dynamical Magnetic Field in van der Waals Bilayers Induced by Light. *Phys. Rev. Lett.* **2024**, *133*, No. 126801.
(24) Yang, Q.; Meng, S. Light-Induced Complete Reversal of Ferroelectric Polarization in Sliding Ferroelectrics. *Phys. Rev. Lett.* **2024**, *133*, No. 136902.
(25) Sie, E. J.; Nyby, C. M.; Pemmaraju, C. D.; Park, S. J.; Shen, X.; Yang, J.; Hoffmann, M. C.; Ofori-Okai, B. K.; Li, R.; Reid, A. H.; et al. An ultrafast symmetry switch in a Weyl semimetal. *Nature* **2019**, *565*, 61−66.
(26) Zeiger, H. J.; Vidal, J.; Cheng, T. K.; Ippen, E. P.; Dresselhaus, G.; Dresselhaus, M. S. Theory for displacive excitation of coherent phonons. *Phys. Rev. B* **1992**, *45*, 768−778.
(27) Faure, J.; Mauchain, J.; Papalazarou, E.; Marsi, M.; Boschetto, D.; Timrov, I.; Vast, N.; Ohtsubo, Y.; Arnaud, B.; Perfetti, L. Direct observation of electron thermalization and electron-phonon coupling in photoexcited bismuth. *Phys. Rev. B* **2013**, *88*, No. 075120.
(28) Zhang, S.; Yan, Z.; Li, Y.; Chen, Z.; Zeng, H. Atomically Thin Arsenene and Antimonene: Semimetal−Semiconductor and Indirect−Direct Band-Gap Transitions. *Angew. Chem., Int. Ed.* **2015**, *54*, 3112−3115.
(29) Xiao, C.; Wang, F.; Yang, S. A.; Lu, Y.; Feng, Y.; Zhang, S. Elemental Ferroelectricity and Antiferroelectricity in Group-V Monolayer. *Adv. Funct. Mater.* **2018**, *28*, No. 1707383.
(30) Gou, J.; Bai, H.; Zhang, X. L.; Huang, Y. L.; Duan, S. S.; Ariando, A.; Yang, S. Y. A.; Chen, L.; Lu, Y. H.; Wee, A. T. S. Two-dimensional ferroelectricity in a single-element bismuth monolayer. *Nature* **2023**, *617*, 67.
(31) Meng, S.; Kaxiras, E. Real-time, local basis-set implementation of time-dependent density functional theory for excited state dynamics simulations. *J. Chem. Phys.* **2008**, *129*, No. 054110.
(32) Troullier, N.; Martins, J. L. Efficient pseudopotentials for plane-wave calculations. *Phys. Rev. B* **1991**, *43*, 1993−2006.
(33) Perdew, J. P.; Burke, K.; Ernzerhof, M. Generalized Gradient Approximation Made Simple. *Phys. Rev. Lett.* **1997**, *78*, 1396.
(34) Alonso, J. L.; Andrade, X.; Echenique, P.; Falceto, F.; Prada-Gracia, D.; Rubio, A. Efficient Formalism for Large-Scale Ab Initio Molecular Dynamics based on Time-Dependent Density Functional Theory. *Phys. Rev. Lett.* **2008**, *101*, No. 096403.
(35) Guo, F.-W.; Liu, W.-H.; Wang, Z.; Li, S.-S.; Wang, L.-W.; Luo, J.-W. Photoinduced hidden monoclinic metallic phase of VO_2 driven by local nucleation. *Nat. Commun.* **2025**, *16*, 94.
(36) Guan, M.; Chen, D.; Chen, Q.; Yao, Y.; Meng, S. Coherent Phonon Assisted Ultrafast Order-Parameter Reversal and Hidden Metallic State in Ta_2NiSe_5. *Phys. Rev. Lett.* **2023**, *131*, No. 256503.
(37) Liu, W.-H.; Gu, Y.-X.; Wang, Z.; Li, S.-S.; Wang, L.-W.; Luo, J.-W. Origin of Immediate Damping of Coherent Oscillations in Photoinduced Charge-Density-Wave Transition. *Phys. Rev. Lett.* **2023**, *130*, No. 146901.
(38) Guan, M. X.; Wang, E.; You, P. W.; Sun, J. T.; Meng, S. Manipulating Weyl quasiparticles by orbital-selective photoexcitation in WTe_2. *Nat. Commun.* **2021**, *12*, 1885.
(39) Xu, C.; Jin, C.; Chen, Z.; Lu, Q.; Cheng, Y.; Zhang, B.; Qi, F.; Chen, J.; Yin, X.; Wang, G.; et al. Transient dynamics of the phase transition in VO_2 revealed by mega-electron-volt ultrafast electron diffraction. *Nat. Commun.* **2023**, *14*, 1265.
(40) Ning, H.; Mehio, O.; Buchhold, M.; Kurumaji, T.; Refael, G.; Checkelsky, J. G.; Hsieh, D. Signatures of Ultrafast Reversal of Excitonic Order in Ta_2NiSe_5. *Phys. Rev. Lett.* **2020**, *125*, No. 267602.
(41) Frigge, T.; Hafke, B.; Witte, T.; Krenzer, B.; Streubühr, C.; Samad Syed, A.; Mikšić Trontl, V.; Avigo, I.; Zhou, P.; Ligges, M.; et al. Optically excited structural transition in atomic wires on surfaces at the quantum limit. *Nature* **2017**, *544*, 207−211.
(42) Ma, W.; Zhang, J.; Yan, L.; Jiao, Y.; Gao, Y.; Meng, S. Recent progresses in real-time local-basis implementation of time dependent density functional theory for electron−nucleus dynamics. *Comput. Mater. Sci.* **2016**, *112*, 478−486.
(43) Chen, N.-K.; Li, X.-B.; Bang, J.; Wang, X.-P.; Han, D.; West, D.; Zhang, S.; Sun, H.-B. Directional Forces by Momentumless Excitation and Order-to-Order Transition in Peierls-Distorted Solids: The Case of GeTe. *Phys. Rev. Lett.* **2018**, *120*, No. 185701.
(44) Qi, Y.; Chen, N.; Vasileiadis, T.; Zahn, D.; Seiler, H.; Li, X.; Ernstorfer, R. Photoinduced Ultrafast Transition of the Local Correlated Structure in Chalcogenide Phase-Change Materials. *Phys. Rev. Lett.* **2022**, *129*, No. 135701.
(45) Gajdoš, M.; Hummer, K.; Kresse, G.; Furthmüller, J.; Bechstedt, F. Linear optical properties in the projector-augmented wave methodology. *Phys. Rev. B* **2006**, *73*, No. 045112.
(46) Kresse, G.; Furthmüller, J. Efficiency of ab-initio total energy calculations for metals and semiconductors using a plane-wave basis set. *Comput. Mater. Sci.* **1996**, *6*, 15−50.
(47) Grimme, S. Semiempirical GGA-type density functional constructed with a long-range dispersion correction. *J. Comput. Chem.* **2006**, *27*, 1787−1799.
(48) Chen, N.-K.; Bang, J.; Li, X.-B.; Wang, X.-P.; Wang, D.; Chen, Q.-D.; Sun, H.-B.; Zhang, S. Optical subpicosecond nonvolatile

https://doi.org/10.1021/acs.nanolett.5c02237
Nano Lett. XXXX, XXX, XXX−XXX

switching and electron-phonon coupling in ferroelectric materials. *Phys. Rev. B* **2020**, *102*, No. 184115.
(49) Wang, G.; Pandey, R.; Karna, S. P. Atomically Thin Group V Elemental Films: Theoretical Investigations of Antimonene Allotropes. *ACS Appl. Mater. Interfaces* **2015**, *7*, 11490−11496.
(50) Shi, Z. Q.; Li, H.; Xue, C. L.; Yuan, Q. Q.; Lv, Y. Y.; Xu, Y. J.; Jia, Z. Y.; Gao, L.; Chen, Y.; Zhu, W.; et al. Tuning the Electronic Structure of an α-Antimonene Monolayer through Interface Engineering. *Nano Lett.* **2020**, *20*, 8408−8414.
(51) Li, J.; Yang, X.; Liu, Y.; Huang, B.; Wu, R.; Zhang, Z.; Zhao, B.; Ma, H.; Dang, W.; Wei, Z.; et al. General synthesis of two-dimensional van der Waals heterostructure arrays. *Nature* **2020**, *579*, 368−374.
(52) Liao, M.; Nicolini, P.; Du, L.; Yuan, J.; Wang, S.; Yu, H.; Tang, J.; Cheng, P.; Watanabe, K.; Taniguchi, T.; et al. Ultra-low friction and edge-pinning effect in large-lattice-mismatch van der Waals heterostructures. *Nat. Mater.* **2022**, *21*, 47−53.

https://doi.org/10.1021/acs.nanolett.5c02237
Nano Lett. XXXX, XXX, XXX−XXX